

Journal of Materials Chemistry A

Accepted Manuscript



This is an *Accepted Manuscript*, which has been through the Royal Society of Chemistry peer review process and has been accepted for publication.

Accepted Manuscripts are published online shortly after acceptance, before technical editing, formatting and proof reading. Using this free service, authors can make their results available to the community, in citable form, before we publish the edited article. We will replace this *Accepted Manuscript* with the edited and formatted *Advance Article* as soon as it is available.

You can find more information about *Accepted Manuscripts* in the [Information for Authors](#).

Please note that technical editing may introduce minor changes to the text and/or graphics, which may alter content. The journal's standard [Terms & Conditions](#) and the [Ethical guidelines](#) still apply. In no event shall the Royal Society of Chemistry be held responsible for any errors or omissions in this *Accepted Manuscript* or any consequences arising from the use of any information it contains.



Journal Name

ARTICLE

Highly Porous Graphitic Carbon and Ni₂P₂O₇ for High Performance Aqueous Hybrid Supercapacitor

Received 00th January 20xx,
Accepted 00th January 20xx

DOI: 10.1039/x0xx00000x

www.rsc.org/

Baskar Senthilkumar,^{†a} Ziyauddin Khan,^{†a} Seungyoung Park,^a Kyoungho Kim,^a Hyunhyub Ko^{*a} and Youngsik Kim^{*a}

An aqueous Na-ion based hybrid capacitor has been successfully developed by highly porous graphitic carbon (HPGC) derived by waste writing paper and a new electrode material as negative and positive electrode, respectively. HPGC was prepared *via* hydrothermal carbonization and subsequent KOH activation of waste writing paper which showed highly porous stacked sheet like morphology with exceptionally high BET specific surface area (1254 m² g⁻¹). HPGC exhibited typical electrical double layer capacitor (EDLC) behavior with a high specific capacitance of 384 F g⁻¹ and good negative working potential (-1.0 V) in aqueous electrolyte. On the other hand, Ni₂P₂O₇ was synthesized by simple co-precipitation technique and tested as cathode material which delivered a maximum specific capacitance of 1893 F g⁻¹ at 2 A g⁻¹ current density. The fabricated HPGC|Ni₂P₂O₇ hybrid device displayed excellent cyclic stability up to 2000 cycles and delivered maximum energy density of 65 W h kg⁻¹ at 800 W kg⁻¹ power density in Na-ion based aqueous electrolyte.

Introduction

Supercapacitors are considered one of the most reliable energy storage devices mainly due to their capability of providing high power (10 kW kg⁻¹), fast charge-discharge kinetics and excellent cycling ability in contrast to the secondary batteries.¹⁻³ Supercapacitors can complement or even replace secondary batteries when high power required such as backups or auxiliary power sources for electric vehicles and electronic devices. However, supercapacitors display low energy density than batteries due to low discharge time, whereas practical applications clearly require more discharge time.⁴

In recent times, hybrid capacitors (HCs) have been emerged as an alternative energy storage devices to achieve higher energy density demand.⁵⁻⁹ A HC is the combination of a capacitive electrode with a battery electrode which can act as a bridge between supercapacitors and batteries.² The performance of the HCs for practical applications depend on the performance of capacitive and battery electrodes in terms of specific capacitance, energy density, power density, rate capability, cyclic stability as well as cost and environment. Much efforts have been devoted to recognize good electrode materials for HCs specially to improve the energy density without sacrificing power density and cyclic stability.

Ruthenium oxide has been in focus as positive electrode

since long due to its highly reversible redox reactions and wide operating electrochemical window^{10, 11} but high cost and toxicity hampers its use for practical applications. In recent years, nickel based materials (NiO, Ni(OH)₂, NiCo₂O₄, NiFe₂O₄, NiMoO₄, Ni₃(PO₄)₂ and Ni₂P₂O₇, etc) have been considered as fascinating battery electrode materials for hybrid capacitors due to low cost, high capacitance and environment friendly.¹²⁻²² Though pyrophosphate materials (Co₂P₂O₇, Mn₂P₂O₇ and Ni₂P₂O₇) have captivated the attention from researcher worldwide,²²⁻²⁵ however, there is only one recent study on nickel pyrophosphate (Ni₂P₂O₇) reported by Wei et al. They synthesized hexagonal tablets of sodium doped Ni₂P₂O₇ by hydrothermal method which delivers its maximum capacitance 557.7 F g⁻¹ at 1.2 A g⁻¹.²² It is worth to mention, though they made high surface area hexagonal tablet but still the capacitance value is low. Herein, we have synthesized Ni₂P₂O₇ by cost-effective and facile precipitation method which delivered its maximum specific capacitance of 1893 F g⁻¹ at 2 A g⁻¹ in aqueous NaOH electrolyte. In addition, 1863 F g⁻¹ capacitance was calculated for 750th cycle demonstrating the excellent cycling stability of Ni₂P₂O₇.

In order to construct a HC, negative electrode is also plays equally important role as positive electrode. Carbonaceous materials like graphene, nanotubes (CNTs) and biomass derived carbon have been predominantly utilized due to complementary electrochemical window.^{18, 26-30} Among them biomass derived carbon has been found attractive anode material due to its low cost, facile synthesis *via* simple pyrolysis or hydrothermal methods and tailored pore size which helps to improve the specific capacitance and eventually energy density of the device.^{29, 31, 32} Wang et al. have reported capacitive electrode by hemp carbonization and assembled

^a School of Energy & Chemical Engineering, Ulsan National Institute of Science and Technology (UNIST), UNIST-gil 50, Ulsan, 689-798, Republic of Korea. Email: ykim@unist.ac.kr; hyunhko@unist.ac.kr

[†] These authors contributed equally to this work.

Electronic Supplementary Information (ESI) available. See DOI: 10.1039/x0xx00000x

supercapacitors device delivers maximum 12 Wh kg^{-1} energy density.²⁹ Ren et al. have synthesized MnO_2 loaded carbonaceous aerogel by hydrothermal carbonization of watermelon which shows maximum 123.5 F g^{-1} specific capacitance.³³ Based on above consideration, we have carbonized the writing/printing paper and converted to HPGC by performing KOH activation step. The prepared HPGC exhibit its maximum specific capacitance 384 F g^{-1} at 4 A g^{-1} current density, excellent rate capability (retained capacitance at high current densities ranging 4 to 20 A g^{-1}) and cyclic stability up to 1500 cycle.

After single electrode performance examination, we report a cost-effective hybrid device delivering maximum energy density of 65 Wh kg^{-1} at 800 W kg^{-1} power density and long cycle life up to 1500 cycles in aqueous NaOH electrolyte, which is built of $\text{Ni}_2\text{P}_2\text{O}_7$ as a positive electrode and HPGC as a negative electrode. For better understanding of current status of HCs with various electrode materials, their energy density is compared as shown in Fig 1.^{14-16, 34-36} For example, Salunkhe et al have demonstrated a hybrid device by the combination of *o*-CNT/ $\text{Ni}(\text{OH})_2$ (*o*-CNT refers to oxidized CNT for better hydrophilicity) as positive material and rGO (reduced graphene oxide) as negative electrode.¹⁵ Though they achieved 1807 W kg^{-1} of maximum power density for the device but the energy density is still low (35.24 Wh kg^{-1}). Gao et al have fabricated a HC by combining porous graphene paper (PGP) as negative electrode and hierarchical NiCo_2O_4 on carbon cloth as positive electrode. The device delivered its maximum energy density of 60.9 Wh kg^{-1} at 11360 W kg^{-1} of power density.¹⁸ Thus we believe that our study could provide new way to fabricate cost effective aqueous Na-ion based hybrid capacitor device by the exploration of new electrode material and laboratory made graphitic carbon by waste paper.

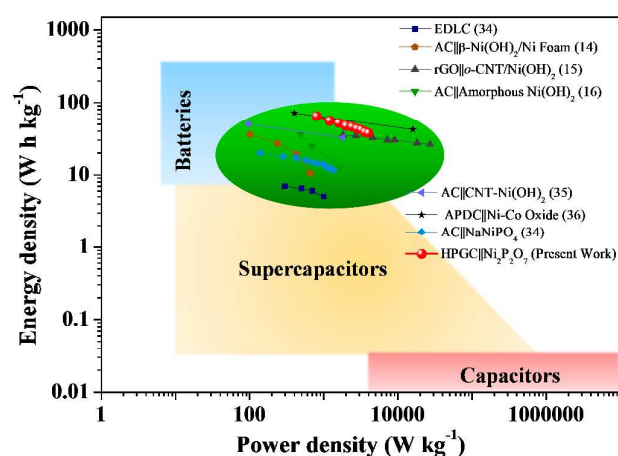


Fig. 1 Comparative Ragone plot for hybrid capacitors with batteries and supercapacitors.³⁷

Results and discussion

Morphology and surface area study of HPGC

In the exploration for appropriate and cost-effective negative electrode for aqueous Na-ion hybrid capacitor we have rationally synthesized high surface area graphitic carbon by

hydrothermal carbonization followed by KOH activation of waste paper as shown in synthetic scheme Fig 2a. The surface morphology of the prepared HPGC was investigated by FE-SEM and compared its morphology with waste paper and carbonized product after hydrothermal treatment (Fig. 1 b-c and *Electronic Supplementary Information* (ESI) Fig S1). At low magnification highly agglomerated and wrinkled stacked sheet like morphology can be seen in ESI Fig S2. However, in high magnification image (Fig 2b & c) highly porous and well interconnected HPGC was observed which was also well supported by TEM analysis (Fig 2d and ESI S3). The formation of highly porous structure could be attributed to the KOH activation step which involves melting and penetration of KOH into the sheet at $800 \text{ }^\circ\text{C}$ heating under Ar atmosphere.³⁸ The elemental mapping of HPGC was also carried out which confirmed presence of carbon element (Fig 2e). In order to calculate the surface area of the HPGC, the N_2 adsorption-desorption experiment was also performed as shown in Fig 2f. According to the Brunauer–Deming–Deming–Teller (BDDT) classification,³⁹ the majority of physisorption isotherms can be grouped into six types according to which sample display typical type-IV isotherms and type H1 hysteresis loop which means HPGC is mesoporous material and distribution of pore size is regular. As measured, HPGC shows exceptionally high BET surface area of value $1254 \text{ m}^2 \text{ g}^{-1}$ and the pore volume vs pore diameter plot (inset Fig 2f) displays that 4 nm pore diameter has highest pore volume.

Phase characterization and chemical composition study of HPGC

Fig 3a shows the X-ray diffraction pattern of prepared HPGC display two broad peak around 26° and 43° correspond to (002) and (100) reflections, respectively, which reveals the formation of graphitic domain during carbonization process. However, peak around 16° could be due to surface oxidation of HPGC. The low intensity and broadened peaks indicate the existence of lattice defects in formed HPGC.⁴⁰ Raman spectroscopy analysis was also performed to further investigate the graphitic nature of prepared carbon which is shown in Fig 3b and ESI Fig. S4. The Raman spectrum of prepared HPGC exhibit D-band (1355 cm^{-1}) and G-band (1588 cm^{-1}) and the relative intensity of G-band is significantly higher compare to D-band ($I_G/I_D = 1.38$) which indicate that prepared HPGC is graphitized.^{41, 42} Further, the chemical bonding state of HPGC was confirmed in detail by XPS as shown in Fig 3c-e. The XPS survey scan suggests the presence of C and O element in HPGC (Fig 3c). The deconvoluted C1s spectra (Fig 3d) provides detailed information about functional groups present in HPGC which includes non-oxygenated ring C=C major peak at binding energy 284.2 eV , the hydroxyl carbon at 285.9 eV , the carbonyl carbon (C=O) at 287.6 eV and the carboxylate carbon (O-C=O) at 289.2 eV .⁴³ The O 1s spectra (Fig 3e) show three deconvoluted peaks at 530.7 , 532.5 and 534.8 eV which is ascribed to physically absorbed oxygen, double bonded oxygen (in acids and esters; O=C-OR) and single bonded oxygen (in acids and esters; RO-C=O), respectively.^{44, 45} The C 1s and O 1s XPS spectra indicate presence of graphitic carbon as well as

other functional group which might be due to the surface oxidation of HPGC also supported by the X-ray diffractogram and Raman spectrum.

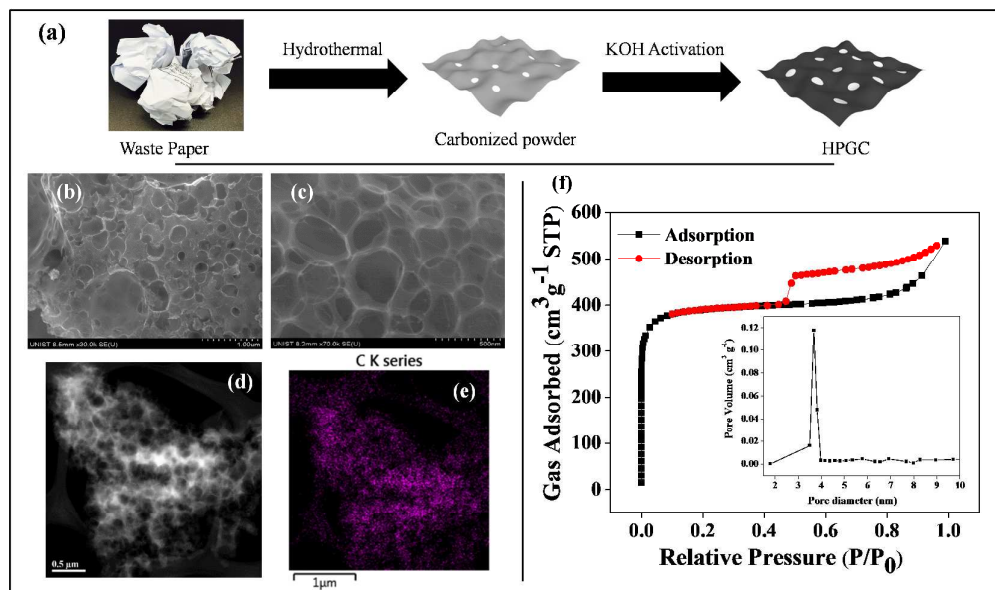


Fig. 2 (a) Synthetic scheme (b) & (c) high magnification SEM images (d) TEM image (e) elemental mapping of HPGC. (f) Nitrogen adsorption-desorption isotherm (inset pore volume vs pore diameter plot) of prepared HPGC.

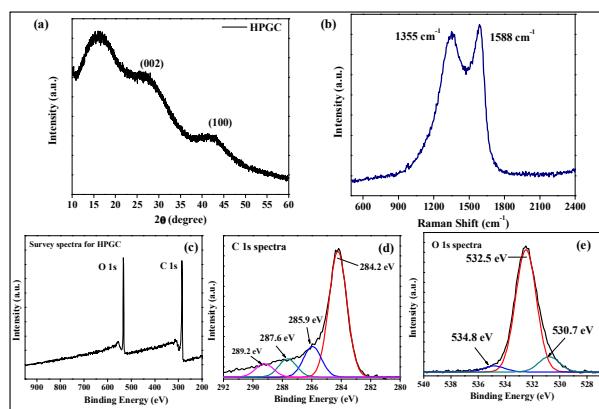


Fig. 3 (a) Powder X-ray diffractogram (b) Raman spectra (c) survey scan (d) C 1s (e) O 1s XPS spectra of HPGC

Electrochemical performance of HPGC

The HPGC derived from waste paper with mesopores and high surface area is expected to display exceptional electrochemical capacitive properties. CV was utilized to evaluate the electrochemical behavior of HPGC in aqueous NaOH electrolyte with Pt counter and Hg/HgO reference electrode and compare its performance with commercial activated carbon (Fig 4a). HPGC gives higher current and improved EDLC behaviour than activated carbon when scan both at 50 mV s⁻¹ from 0.0 to -1.0 V which could be due to highly porous nature of HPGC. Therefore, it would be concluded that waste paper derived HPGC can be a good candidate for EDLC as anode

material in contrast to activated carbon. Fig 4b shows the CV plot for HPGC as anode at different scan rates ranging from 10 to 200 mV s⁻¹ which displays the quasi rectangle shape, characteristics of a typical EDLC, even at high scan rate of 200 mV s⁻¹. The electrochemical capacitance of HPGC was evaluated by galvanostatic charge-discharge profile. The charge-discharge curves (Fig 4c), at different current densities ranging from 4 to 20 A g⁻¹ between voltage window 0.0 and -1.0 V appeared to be symmetric inverted V-shape which also insinuates EDLC nature of HPGC. An electrochemisorption of electrolyte cations (Na⁺) at the negative electrode (HPGC), with the formation of electrical double layer facilitate the charge storage process. Remarkably, the calculated specific capacitance (384 F g⁻¹) was found constant at different current density up to 20 A g⁻¹ which ascribe the outstanding rate capability of active material. This noteworthy behavior could be attributed to the excellent diffusion of electrolyte ions into the electroactive materials due to high surface area and mesoporous nature of HPGC. Moreover, small IR drop was observed during charge-discharge which indicates high electrical conductivity of HPGC electrode resulting high performance electrode. It is also worthy to mention here that the presence of functional groups on HPGC can greatly increase its hydrophilicity resulting ions adsorption improvement in aqueous electrolyte which could also contribute in the excellent performance of HPGC.⁴⁶ We have also performed 1500 cycles charge-discharge at 4 A g⁻¹ for HPGC in order to investigate its cyclic stability as shown in Fig 4d. Notably, it was observed that HPGC absolutely retains its initial specific capacitance up to 1500 cycles which is an ultimate behavior of EDLC. SEM analysis was carried out for

HPGC after 1500 charge-discharge cycle which is shown in ESI Fig S6. No significant change in morphology was observed which also implies that only electrochemisorption of Na^+ ion takes place at HPGC electrode. The excellent electrochemical behavior of HPGC is due to the high surface area, retained morphology and good electronic conductivity.

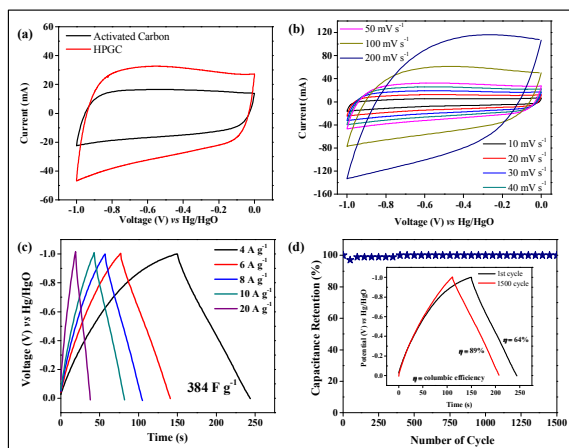


Fig. 4 Electrochemical behavior of prepared HPGC in aqueous electrolyte with Pt counter and Hg/HgO reference electrode (a) comparison with commercial available activated carbon at 50 mV s^{-1} scan rate (b) CV curves at different scan rates; (c) Galvanostatic charge-discharge profile at different current density and (d) cyclic stability test up to 1500 cycles at 4 A g^{-1} current density (inset shows charge-discharge profile of HPGC at first cycle and 1500 cycle)

Phase purity and chemical bonding analyses of $\text{Ni}_2\text{P}_2\text{O}_7$

To build a practical Na-ion based hybrid capacitor device, it is also required to find a suitable positive electrode which should have sufficient working potential and reversibility. More than decade, various nickel based system have been studied as positive electrode which displayed good working potential (0.45 V) and highly reversible redox reaction in aqueous alkali electrolytes.^{16, 20, 47} Herein, we have synthesized $\text{Ni}_2\text{P}_2\text{O}_7$ by facile precipitation method followed by calcination in air. The phase formation temperature of the prepared $\text{Ni}_2\text{P}_2\text{O}_7$ was determined by thermogravimetric analysis (TGA) experiment. TGA of $\text{Ni}_2\text{P}_2\text{O}_7$ was carried out in a static air atmosphere at a heating rate of $10 \text{ }^\circ\text{C}$ per minute and analysis of as prepared sample show one step weight loss about 23 % at $800 \text{ }^\circ\text{C}$ (ESI Fig S7a). The weight loss is assigned to the removal of structure water molecules. Further no significant weight loss is observed which substantiating the formation of pure phase. The phase formation of $\text{Ni}_2\text{P}_2\text{O}_7$ at different calcination temperature was also examined by powder X-ray diffractogram (PXRD) as shown in Fig 5a. The observed pattern in PXRD affirms that pure phase $\text{Ni}_2\text{P}_2\text{O}_7$ formed at $800 \text{ }^\circ\text{C}$ which is well matched with JCPDS card number 74-1604. This confirms the formation of monoclinic phase pure $\text{Ni}_2\text{P}_2\text{O}_7$ with a space group of B21/c. However, there was no significant change observe between as prepared sample (without calcination) and the sample calcined at $600 \text{ }^\circ\text{C}$. The chemical bonding in $\text{Ni}_2\text{P}_2\text{O}_7$ was determined by X-ray photoelectron spectroscopy (XPS) as shown in ESI Fig S7b-e. Fig S7b shows XPS survey spectra of $\text{Ni}_2\text{P}_2\text{O}_7$ and

obtained peaks confirm the presence of Ni, O and P elements. In high resolution spectrum of Ni 2p, two peaks centred at 875.1 and 856.6 eV corresponding to Ni $2p_{3/2}$ and Ni $2p_{1/2}$ are identified (Fig S7c). Along with this two satellite peaks, at 861.7 and 879.8 eV, were also observed.⁴⁸ The O1s spectra (Fig S7d) confirms the presence of metal oxide (M-O; 532.6 eV).⁴⁹ However, the peaks observed at 133.5 and 135.8 eV in high resolution spectrum of P 2p (Fig S7e) is assigned to P $2p_{3/2}$ and P $2p_{1/2}$.

Surface morphology and surface area study of $\text{Ni}_2\text{P}_2\text{O}_7$

The surface morphology of $\text{Ni}_2\text{P}_2\text{O}_7$ was examined by FE-SEM which shows that particles have uniform grain-like morphology with high agglomeration and size of particles varies from 200-300 nm also supported by TEM analysis (Fig 5b-d). Figure 5e displays an energy-dispersive X-ray (EDX) pattern for $\text{Ni}_2\text{P}_2\text{O}_7$ which confirms the presence of Ni, P and O elements and the observed atomic ratio of Ni, P and O are matched with the stoichiometry of the $\text{Ni}_2\text{P}_2\text{O}_7$ compound (ESI Table S1). Elemental mapping of $\text{Ni}_2\text{P}_2\text{O}_7$ sample was also carried out as shown in Fig 5f-i, confirms the presence and uniform distribution of Ni, P and O elements. The BET surface area of $\text{Ni}_2\text{P}_2\text{O}_7$ was measured by nitrogen adsorption desorption experiment shown in Fig 5j which was calculated to be $6 \text{ m}^2 \text{ g}^{-1}$ and mesopores formation is identified by average measured pore width of 11 nm (BJH method). The pores of the material can facilitate diffusion of electrolyte ions (OH^-) and redox reaction with increase in active electrode area.^{12, 13, 50}

Electrochemical performance of $\text{Ni}_2\text{P}_2\text{O}_7$

The prepared monoclinic phase pure $\text{Ni}_2\text{P}_2\text{O}_7$ was tested as positive electrode material for the first time in aqueous alkali electrolyte. CV curves of $\text{Ni}_2\text{P}_2\text{O}_7$ in NaOH electrolyte recorded at a scan rate of 5 mV s^{-1} is shown in Fig 6a. The oxidation peak is observed at 0.45 V and corresponding reduction peak at 0.33 V vs Hg/HgO. The redox peaks is assigned to the diffusion controlled reversible redox reaction of $\text{Ni(II)} \leftrightarrow \text{Ni(III)}$ reaction.^{16, 20} In the first cycle the anodic (cathodic) peak current value is 5 mA which increases with number of cycle and reaches $\sim 70 \text{ mA}$ as shown in Fig 6a. The increase in peak current value is due the activation process of the $\text{Ni}_2\text{P}_2\text{O}_7$ electrode material. The peak current values get saturated above 400 cycles, subsequently the CV tests are performed for different scan rates to investigate the rate capability of active material shown in Fig 6b. The redox peaks are reproducible in high scan rates substantiating the rapid electronic transport of the material in the given scan rates.¹⁶ Galvanostatic charge-discharge measurements are also carried out to calculate the specific capacitance in various scan rates (Fig 6c). The curves show plateau regions in 0.45 and 0.33 V vs Hg/HgO which is due to the following reversible redox reaction (1).



The prepared $\text{Ni}_2\text{P}_2\text{O}_7$ showed a maximum specific capacitance of 1893 F g^{-1} at 2 A g^{-1} current density which is higher to other Ni-based double metal oxides such as Ni-Co oxide (1846 F g^{-1}),³⁶ NiMoO_4 (1517 F g^{-1}),²⁰ NiWO_4 (586.2 F g^{-1}),⁵¹ NiCo_2O_4 (895 F g^{-1}),^{17, 52} NaNiPO_4 (368 F g^{-1}),³⁴

$\text{Na}_4\text{Ni}_3(\text{PO}_4)_2\text{P}_2\text{O}_7$ (584 F g^{-1})²¹. The capacitance of 1157 F g^{-1} was observed even at high current density of 10 A g^{-1} confirms the good rate capability of active material. The cycling stability of the $\text{Ni}_2\text{P}_2\text{O}_7$ is tested up to 750 cycles with various current

densities (Fig 6d). Please note that no significant change in initial capacitance was

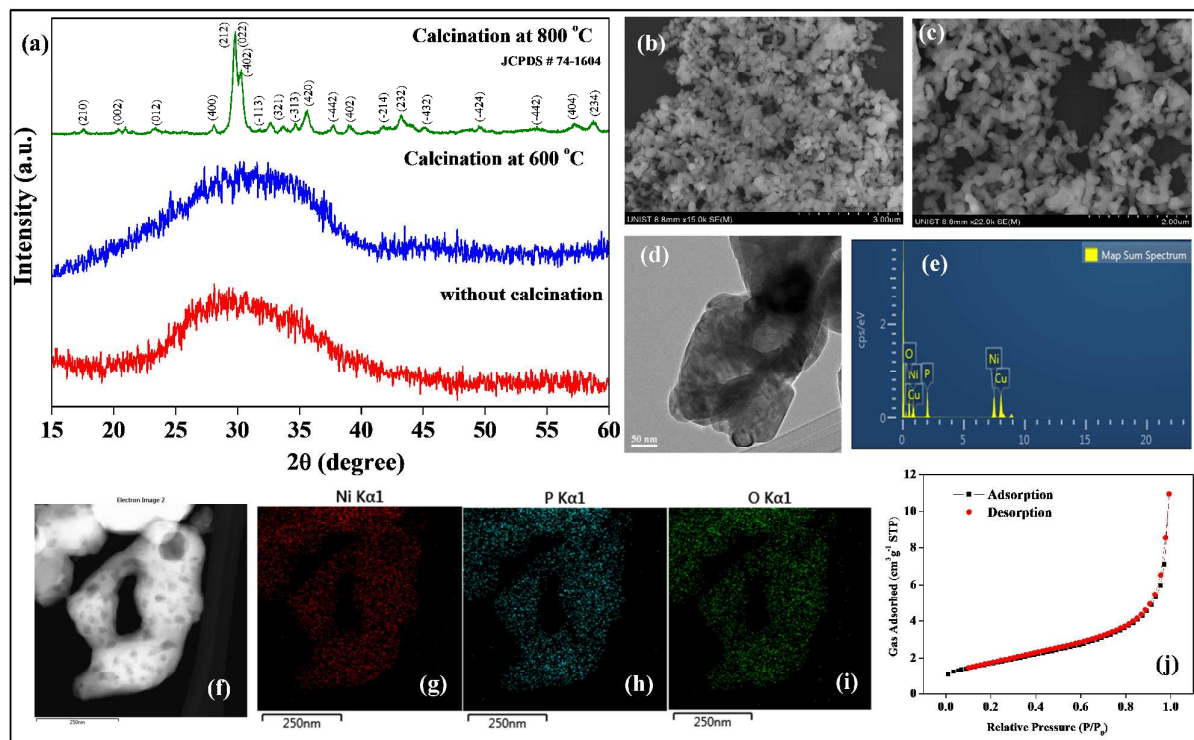


Fig. 5 (a) Powder X-ray diffraction pattern for without calcined and calcined samples at 600 & 800 °C (b) & (c) SEM images; (d) TEM image of $\text{Ni}_2\text{P}_2\text{O}_7$; (e) energy-dispersive X-ray pattern, elemental mapping (f) mapped area and presence of (g) Ni element (h) P element and (i) O element (j) Nitrogen adsorption-desorption isotherm of $\text{Ni}_2\text{P}_2\text{O}_7$.

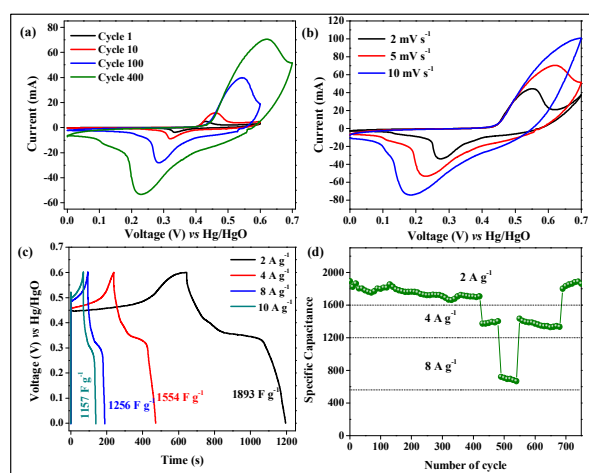


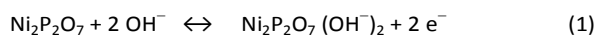
Fig. 6 Electrochemical behavior of $\text{Ni}_2\text{P}_2\text{O}_7$ in aqueous electrolyte with Pt counter and Hg/HgO reference electrode (a) and (b) are CV curves at 5 mV s^{-1} for 1st, 10th, 100 & 400 cycle and at three different scan rates; (c) Galvanostatic charge-discharge profile at different current density and (d) cyclic stability test up to 750 cycles at different current density.

observed during cycling stability test. The initial capacitance was almost retained (1863 F g^{-1}) even after testing at different current densities which validate the outstanding cycling stability of $\text{Ni}_2\text{P}_2\text{O}_7$. To understand the outstanding capacitive feature of the material the surface morphology was examined after 750 charge-discharge cycles (ESI Fig S9). Unlike HPGC, the morphology of the samples changed from grains to more open and porous flake-like morphology which could be accredited to the intercalation of OH^- ions to positive electrode.

Performance study of hybrid capacitor (HPGC | $\text{Ni}_2\text{P}_2\text{O}_7$)

Based on the above electrochemical results, a hybrid supercapacitor device is fabricated using $\text{Ni}_2\text{P}_2\text{O}_7$ and HPGC as positive and negative electrode, respectively. The schematic illustration of hybrid device and proposed charge storage mechanism is shown in Scheme 1. The recorded CV curves for hybrid device at various scan rates are shown in Fig 7a. The oxidation-reduction peaks observed in CV curves are due to the electrochemical redox behaviour of Ni. However, the electrochemical reaction in the electrodes of the cell is shown below:

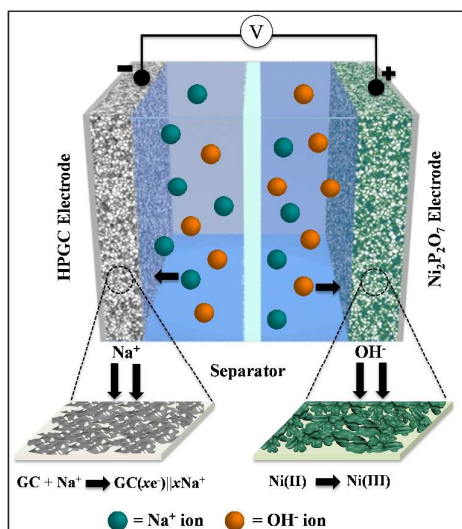
At positive electrode



At negative electrode



(here, || indicates electrical double layer)



Scheme 1 Schematic representation of hybrid device made by waste paper derived HPGC and $\text{Ni}_2\text{P}_2\text{O}_7$ as anode and cathode in charged state in aqueous Na ion electrolyte.

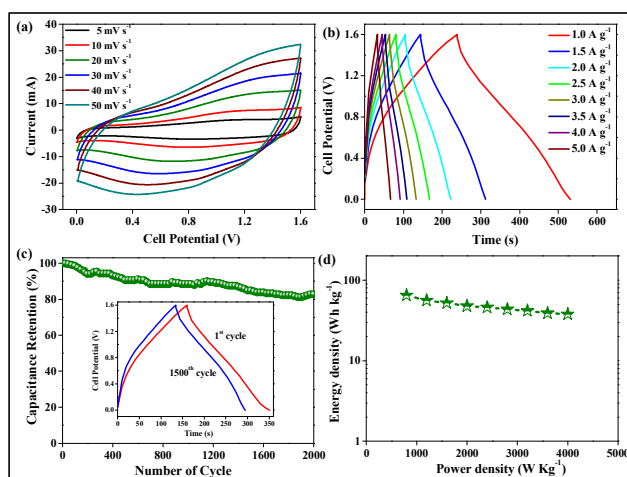
During charge storage process, OH^- ions are intercalating to the $\text{Ni}_2\text{P}_2\text{O}_7$ however, Na^+ ions are chemisorbed on the surface of mesoporous HPGC. The galvanostatic charge-discharge behavior of the hybrid device at different current densities ranging from 1.0 A g^{-1} to 5.0 A g^{-1} is shown in Fig 7b. The curves show quasi-symmetric charge-discharge behavior owing to the intercalation of OH^- ions which also corroborates the CV results (Fig 7a). The cycling stability of the hybrid device is also tested up to 2000 cycles for long term performance (Fig 7c) and it was observed that device retains $\sim 83\%$ of its initial value up to 2000 cycles.

Fig. 7 (a) CV curves at different scan rates; (b) Galvanostatic charge-discharge profile at different current density (c) long term cyclic performance (inset shows charge-discharge profile of full cell at first cycle and 2000 cycle) and (d) Ragone plot for HPGC- $\text{Ni}_2\text{P}_2\text{O}_7$ based fabricated device measured in aqueous Na-ion electrolyte.

Fig 7d presents a Ragone plot, which relates the energy density to the power density of the hybrid supercapacitor device. The hybrid Na-ion based device delivered a maximum energy density of 65 W h kg^{-1} at 800 W kg^{-1} power density in 1 M NaOH electrolyte and it is maintained to 38 W h kg^{-1} at high power density of 4000 W kg^{-1} which suggest that this hybrid device has great promise for practical application in terms of stability, cost and environment. The energy density value of the hybrid device is significantly higher than the reported AC|| $\alpha\text{-Ni}(\text{OH})_2$, AC|| NaNiPO_4 and AC|| $\text{NaNi}_{1/3}\text{Co}_{1/3}\text{Mn}_{1/3}\text{PO}_4$ hybrid capacitors. However, for broader context of our work, the energy density of our hybrid device is compared with the other reported Ni based hybrid device shown in Table 1. From Table 1, it can be clearly observed that HPGC|| $\text{Ni}_2\text{P}_2\text{O}_7$ hybrid device shows better performance than most of the AC and metal oxide based hybrid capacitor reported previously in the literature.

Conclusions

In summary, HPGC and a new electrode material $\text{Ni}_2\text{P}_2\text{O}_7$ were synthesized by waste paper and precipitation method, respectively. HPGC and $\text{Ni}_2\text{P}_2\text{O}_7$ were tested as anode and cathode correspondingly *via* half-cell in aqueous electrolyte and found that HPGC and $\text{Ni}_2\text{P}_2\text{O}_7$ can be good electroactive material for aqueous Na-ion based device. We have also successfully fabricated hybrid capacitor built HPGC as anode and $\text{Ni}_2\text{P}_2\text{O}_7$ as cathode and examined its performance in aqueous sodium based electrolyte. The hybrid device showed excellent electrochemical properties of high capacitance, high rate capability and good cycling stability. The hybrid capacitor has the advantages of low cost, environmental benign, high energy density (65 W h kg^{-1}) and good cycling stability. We believe that present study can open up new way to design cost-effective hybrid capacitor by using electrode materials which can be synthesized by waste and without much effort.





Journal Name

ARTICLE

Table 1: Comparison table of prepared hybrid capacitor with reported hybrid capacitors

Hybrid Capacitor	Specific Capacitance (F g ⁻¹)	Energy Density (W h kg ⁻¹)	Power density (W kg ⁻¹)	Cyclic stability		Ref
				Retention	Cycle number	
PGP NiCo ₂ O ₄ /CC ^a	71.32	60.9	11360	96.8	5000	18
AC NiMoO ₄ /CoMoO ₄ .xH ₂ O	80	28	100	92	1000	20
AC NaNiPO ₄	56	20	138	70	500	34
AC β-Ni(OH) ₂ /Ni Foam	105.8	36.2	100.6	92	1000	14
APDC Ni-Co oxide ^b	202	71.7	400	~80	4000	36
rGO σ-CNT/Ni(OH) ₂	78.33	35.24	1807	100	1400	15
AC α-Ni(OH) ₂	127	42.3	110	82	1000	53
AC NiMoO ₄ .xH ₂ O	96.7	34.4	165	~81	1000	54
AC NiCo ₂ O ₄ /rGO	99.4	23.32	324.9	83	2500	55
AC NaNi _{1/3} Co _{1/3} Mn _{1/3} PO ₄	45	15	400	-	1000	56
HPGC Ni ₂ P ₂ O ₇	183	65	800	83	2000	Present work

^a PGP and CC refer to Porous Graphene Paper and Carbon Cloth; ^b APDC refers to Activated Polyaniline-derived Carbon;

Experimental Details**Synthesis of HPGC**

HPGC was synthesized *via* hydrothermal method by carbonization of discarded writing paper followed by activation by KOH. In typical synthesis, 3 g of waste paper (cut in to small pieces) was treated hydrothermally with 50% dilute sulfuric acid (50 mL) at 160 °C for 16 h. After hydrothermal reaction, the autoclave was allowed to cool naturally and obtained product was filtered and washed with water several time to remove excess acid, if present. The product was dried in hot air oven and further grind it prior to KOH activation step in order to get powder form of product. The obtained powder was mixed with KOH (Sigma Aldrich) in 1:1 ratio and annealed at 800 °C for 2 h in argon atmosphere and allowed to cool to room temperature. The resultant powder was then thoroughly washed with 10 wt% HCl (DaeJung Chemicals, Korea) to remove any inorganic impurity and finally wash with water until neutral pH was achieved. The subsequent powder was dried in hot air oven at 60 °C and used for further characterization and supercapacitors experiments.

Synthesis of Ni₂P₂O₇

For the preparation of nickel pyrophosphate, stoichiometric amounts of nickel nitrate Ni(NO₃)₂.6H₂O and ammonium dihydrogen phosphate (NH₄H₂PO₄) were used as precursors. Lithium hydroxide solution (LiOH.H₂O) was used as precipitating agent. The precursors were dissolved in distilled water and stirred overnight in magnetic stirrer. The final precipitate was collected by centrifuge and washed with

distilled water. The sample was dried at 80 °C and calcination was carried out at different temperatures.

Materials Characterization

Crystal structure of the samples were characterized by powder X-ray diffraction (XRD) data which was collected using the Bruker D8 Advance Diffractometer equipped with Cu-Kα radiation and a diffractometer monochromator that was operated at 40 kV and 30 mA. TGA was performed by TA SDT 2960 Simultaneous DSC-TGA instruments. The surface morphologies of the samples were examined by Hitachi, S-4800, Field Emission Scanning Electron Microscopy (FE-SEM) at 10 kV operating voltage. The sample was dispersed in EtOH and put drop onto the silicon wafers, which were positioned over the top of FE-SEM stubs. TEM was performed with JEOL JEM 2100 high-resolution field emission transmission electron microscope, using an accelerating voltage of 200 kV. Energy-dispersive X-ray (EDX) spectroscopic analysis and elemental maps were performed by an INCA, Oxford Instruments attached with HR-TEM. The chemical bonding and functional group was investigated by X-ray Photoelectron Spectrometer (XPS, K-alpha, Thermo Fisher, UK) and confocal Raman microscope (alpha 300R, WITec, Germany) with excitation wavelength at 532 nm. The BET surface areas were analysed by nitrogen (N₂) adsorption at liquid N₂ temperature with a Micromeritics ASAP 2020 nitrogen adsorption apparatus. All the samples were degassed at 120 °C for 12 h prior to the N₂ adsorption measurements.

Electrode preparation and electrochemical measurement

For electrochemical measurement, the active electrodes (HPGC, Ni₂P₂O₇ and AC) were prepared by mixing electroactive material (75 wt %), super P carbon black (20 wt %) and PVDF (5 wt %) with 0.35 mL of NMP to form a slurry which was coated and dried on carbon paper (area of coating, 1 cm²). Cyclic Voltammetry (CV) and galvanostatic charge-discharge studies of the HPGC, Ni₂P₂O₇ and AC half cells were carried out using Ivium Technologies Instruments, Iviumstat. For electrochemical characterization Pt plate as counter and Hg/HgO as reference electrode was used. A full cell (HPGC||Ni₂P₂O₇) was fabricated by using celgard separator. The cyclic voltammetry and galvanostatic charge-discharge studies of the full cell was carried out using Biologic Science Instruments VSP 300 in 1 M NaOH electrolyte at room temperature.

Acknowledgements

This work was supported by the 2015 Research Fund (1.150034.01) of UNIST (Ulsan National Institute of Science and Technology) and development program of the Korea Institute of Energy Research (KIER) (B5-2422).

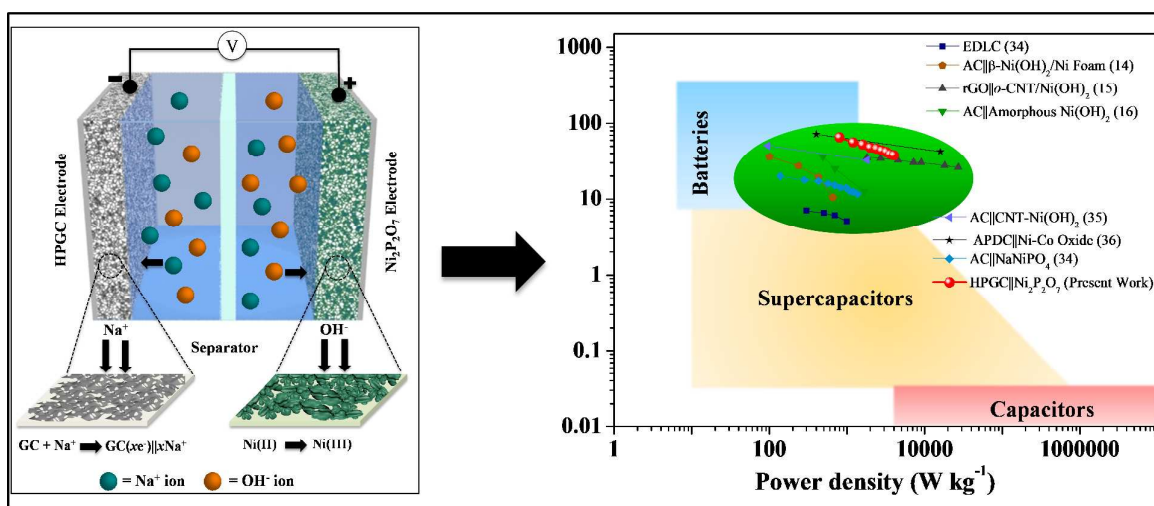
Notes and references

- J. R. Miller and P. Simon, *Science*, 2008, **321**, 651-652.
- P. Simon and Y. Gogotsi, *Nat. Mater.*, 2008, **7**, 845-854.
- A. S. Arico, P. Bruce, B. Scrosati, J. M. Tarascon and W. van Schalkwijk, *Nat. Mater.*, 2005, **4**, 366-377.
- R. Kötz and M. Carlen, *Electrochim. Acta*, 2000, **45**, 2483-2498.
- K. Naoi, *Fuel Cells*, 2010, **10**, 825-833.
- K. Naoi, S. Ishimoto, J. Miyamoto and W. Naoi, *Energy Environ. Sci.*, 2012, **5**, 9363-9373.
- K. Naoi, W. Naoi, S. Aoyagi, J. Miyamoto and T. Kamino, *Acc. Chem. Res.*, 2013, **46**, 1075-1083.
- J. Liu, L. Zhang, H. B. Wu, J. Lin, Z. Shen and X. W. Lou, *Energy Environ. Sci.*, 2014, **7**, 3709-3719.
- L. Li, S. Peng, H. B. Wu, L. Yu, S. Madhavi and X. W. Lou, *Adv. Energy Mater.*, 2015, DOI: 10.1002/aenm.201500753.
- W. Sugimoto, H. Iwata, Y. Yasunaga, Y. Murakami and Y. Takasu, *Angew. Chem. Int. Ed.*, 2003, **42**, 4092-4096.
- C. Yuan, L. Chen, B. Gao, L. Su and X. Zhang, *J. Mater. Chem.*, 2009, **19**, 246-252.
- C. Z. Yuan, X. G. Zhang, L. H. Su, B. Gao and L. F. Shen, *J. Mater. Chem.*, 2009, **19**, 5772-5777.
- M. M. Liu, J. Chang, J. Sun and L. Gao, *Electrochim. Acta*, 2013, **107**, 9-15.
- J. C. Huang, P. P. Xu, D. X. Cao, X. B. Zhou, S. N. Yang, Y. J. Li and G. L. Wang, *J. Power Sources*, 2014, **246**, 371-376.
- R. R. Salunkhe, J. J. Lin, V. Malgras, S. X. Dou, J. H. Kim and Y. Yamauchi, *Nano Energy*, 2015, **11**, 211-218.
- H. B. Li, M. H. Yu, F. X. Wang, P. Liu, Y. Liang, J. Xiao, C. X. Wang, Y. X. Tong and G. W. Yang, *Nat. Commun.*, 2013, **4**, 1894.
- W. W. Zhou, D. Z. Kong, X. T. Jia, C. Y. Ding, C. W. Cheng and G. W. Wen, *J. Mater. Chem. A*, 2014, **2**, 6310-6315.
- Z. Gao, W. Yang, J. Wang, N. Song and X. Li, *Nano Energy*, 2015, **13**, 306-317.
- Z.-Y. Yu, L.-F. Chen and S.-H. Yu, *J. Mater. Chem. A*, 2014, **2**, 10889-10894.
- B. Senthilkumar, D. Meyrick, Y.-S. Lee and R. K. Selvan, *RSC Adv.*, 2013, **3**, 16542-16548.
- B. Senthilkumar, G. Ananya, P. Ashok and S. Ramaprabhu, *Electrochim. Acta*, 2015, **169**, 447-455.
- H. Pang, C. Z. Wei, C. Cheng, S. Wang, Y. Z. Xu and J. D. Wang, *Chem. - Asian J.*, 2015, DOI: 10.1002/asia.201500335.
- L. R. Hou, L. Lian, D. K. Li, J. D. Lin, G. Pan, L. H. Zhang, X. G. Zhang, Q. G. Zhang and C. Z. Yuan, *RSC Adv.*, 2013, **3**, 21558-21562.
- H. Pang, Z. Z. Yan, Y. H. Ma, G. C. Li, J. Chen, J. S. Zhang, W. M. Du and S. J. Li, *J. Solid State Electrochem.*, 2013, **17**, 1383-1391.
- H. Pang, Z. Yan, W. Wang, Y. Wei, X. Li, J. Li, J. Chen, J. Zhang and H. Zheng, *Int. J. Electrochem. Sci.*, 2012, **7**, 12340-12353.
- W. Tang, L. Liu, S. Tian, L. Li, Y. Yue, Y. Wu and K. Zhu, *Chem. Commun.* 2011, **47**, 10058-10060.
- C. Peng, S. W. Zhang, D. Jewell and G. Z. Chen, *Prog. Nat. Sci.*, 2008, **18**, 777-788.
- Z. Khan, S. Bhattu, S. Haram and D. Khushalani, *RSC Adv.*, 2014, **4**, 17378-17381.
- H. Wang, Z. Xu, A. Kohandehghan, Z. Li, K. Cui, X. Tan, T. J. Stephenson, C. K. King'ondeu, C. M. Holt, B. C. Olsen, J. K. Tak, D. Harfield, A. O. Anyia and D. Mitlin, *ACS Nano*, 2013, **7**, 5131-5141.
- M. D. Stoller, S. Park, Y. Zhu, J. An and R. S. Ruoff, *Nano Lett.*, 2008, **8**, 3498-3502.
- L. Wei, M. Sevilla, A. B. Fuertes, R. Mokaya and G. Yushin, *Adv. Energy Mater.*, 2011, **1**, 356-361.
- D. Puthusseri, V. Aravindan, B. Anothumakkool, S. Kurungot, S. Madhavi and S. Ogale, *Small*, 2014, **10**, 4395-4402.
- Y. Ren, Q. Xu, J. Zhang, H. Yang, B. Wang, D. Yang, J. Hu and Z. Liu, *ACS Appl. Mater. Inter.*, 2014, **6**, 9689-9697.
- B. Senthilkumar, K. V. Sankar, L. Vasylechko, Y.-S. Lee and R. K. Selvan, *RSC Adv.*, 2014, **4**, 53192-53200.
- Z. Tang, C. h. Tang and H. Gong, *Adv. Funct. Mater.*, 2012, **22**, 1272-1278.
- R. Wang and X. Yan, *Sci. Rep.*, 2014, **4**, 3712.
- M. Winter and R. J. Brodd, *Chem. Rev.*, 2004, **104**, 4245-4270.
- Y. Zhu, S. Murali, M. D. Stoller, K. J. Ganesh, W. Cai, P. J. Ferreira, A. Pirkle, R. M. Wallace, K. A. Cychosz, M. Thommes, D. Su, E. A. Stach and R. S. Ruoff, *Science*, 2011, **332**, 1537-1541.
- K. S. W. Sing, D. H. Everett, R. A. W. Haul, L. Moscou, R. A. Pierotti, J. Rouquerol and T. Siemieniewska, *Pure Appl. Chem.*, 1985, **57**, 603-619.
- Y. M. Wang, J. Y. Cao, Y. Zhou, J. H. Ouyang, D. C. Jia and L. X. Guo, *J. Electrochem. Soc.*, 2012, **159**, A579-A583.
- Y. Wang, D. C. Alsmeyer and R. L. Mccreery, *Chem. Mater.*, 1990, **2**, 557-563.
- J. Ding, H. Wang, Z. Li, A. Kohandehghan, K. Cui, Z. Xu, B. Zahiri, X. Tan, E. M. Lotfabad, B. C. Olsen and D. Mitlin, *ACS Nano*, 2013, **7**, 11004-11015.
- Y. E. Shin, Y. J. Sa, S. Park, J. Lee, K. H. Shin, S. H. Joo and H. Ko, *Nanoscale*, 2014, **6**, 9734-9741.

44. V. Datsyuk, M. Kalyva, K. Papagelis, J. Parthenios, D. Tasis, A. Siokou, I. Kallitsis and C. Galiotis, *Carbon*, 2008, **46**, 833-840.
45. D. Rosenthal, M. Ruta, R. Schlogl and L. Kiwi-Minsker, *Carbon*, 2010, **48**, 1835-1843.
46. R. J. White, V. Budarin, R. Luque, J. H. Clark and D. J. Macquarrie, *Chem. Soc. Rev.*, 2009, **38**, 3401-3418.
47. G. W. Yang, C. L. Xu and H. L. Li, *Chem. Commun.*, 2008, 6537-6539.
48. R. Moreno-Tost, J. Santamaria-Gonzalez, P. Maireles-Torres, E. Rodriguez-Castellon and A. Jimenez-Lopez, *J. Mater. Chem.*, 2002, **12**, 3331-3336.
49. F. J. Miao, C. L. Shao, X. H. Li, Y. Zhang, N. Lu, K. X. Wang and Y. C. Liu, *Int. J. Hydrogen Energy*, 2014, **39**, 16162-16170.
50. M. Zhu, X. Zhang, Y. Zhou, C. Zhuo, J. Huang and S. Li, *RSC Adv.*, 2015, **5**, 39270-39277.
51. L. Niu, Z. Li, Y. Xu, J. Sun, W. Hong, X. Liu, J. Wang and S. Yang, *ACS Appl. Mater. Interfaces*, 2013, **5**, 8044-8052.
52. J. Zhou, Y. Huang, X. Cao, B. Ouyang, W. Sun, C. Tan, Y. Zhang, Q. Ma, S. Liang, Q. Yan and H. Zhang, *Nanoscale*, 2015, **7**, 7035-7039.
53. J. W. Lang, L. B. Kong, M. Liu, Y. C. Luo and L. Kang, *J. Solid State Electrochem.*, 2010, **14**, 1533-1539.
54. M.-C. Liu, L. Kang, L.-B. Kong, C. Lu, X.-J. Ma, X.-M. Li and Y.-C. Luo, *RSC Adv.*, 2013, **3**, 6472-6478.
55. X. Wang, W. S. Liu, X. H. Lu and P. S. Lee, *J. Mater. Chem.*, 2012, **22**, 23114-23119.
56. M. Minakshi, D. Meyrick and D. Appadoo, *Energy Fuels*, 2013, **27**, 3516-3522.

Graphical Abstract

A high energy hybrid capacitor was fabricated using highly porous graphitic carbon carbonized from discarded writing paper and a novel electrode material $\text{Ni}_2\text{P}_2\text{O}_7$. The hybrid device delivers its maximum energy density 65 W h kg^{-1} at power density 800 W kg^{-1} , good rate capability and cyclic stability in aqueous Na-ion based electrolyte. Our strategy provides a cost-effective and environmental friendly way to fabricate high energy storage device.





Journal Name

ARTICLE

Graphical Abstract

A high energy hybrid capacitor was fabricated using highly porous graphitic carbon carbonized from discarded writing paper and a novel electrode material $\text{Ni}_2\text{P}_2\text{O}_7$. The hybrid device delivers its maximum energy density 65 W h kg^{-1} at power density 800 W kg^{-1} , good rate capability and cyclic stability in aqueous Na-ion based electrolyte. Our strategy provides a cost-effective and environmental friendly way to fabricate high energy storage device

